Journal of Molecular Structure 1143 (2017) 462–471

Contents lists available at ScienceDirect

Journal of Molecular Structure

journal homepage: http://www.elsevier.com/locate/molstruc

Synthesis, characterization, and biological activity of some novel Schiff bases and their Co(II) and Ni(II) complexes: A new route for Co_3O_4 and NiO nanoparticles for photocatalytic degradation of methylene blue dye

Mostafa Y. Nassar*, Hisham M. Aly, Ehab A. Abdelrahman, Moustafa E. Moustafa

Chemistry Department, Faculty of Science, Benha University, Benha, 13518, Egypt

ARTICLE INFO

Article history:
Received 1 March 2017
Received in revised form
28 April 2017
Accepted 29 April 2017
Available online 3 May 2017

Keywords:
Ni(II) and Co(II) Schiff base complexes
Biological activity
Cobalt oxide
Nanoparticles
Nickel oxide
Photocatalytic degradation

ABSTRACT

Six novel Co(II) and Ni(II)-triazole Schiff base complexes have been successfully synthesized by refluxing the prepared triazole Schiff bases with $CoCl_2 \cdot 6H_2O$ or $NiCl_2 \cdot 6H_2O$. The Schiff base ligands were prepared through condensation of 3-R-4-amino-5-hydrazino-1,2,4-triazole with dibenzoylmethane [R=H, CH_3, and CH_2CH_3; namely, L1, L2, and L3, respectively]. The prepared Co(II) and Ni(II) complexes have been identified using elemental analysis, FT-IR, UV–Vis, magnetic moment, conductivity, and thermal analysis. On the basis of the conductance results, it was concluded that all the prepared complexes are non-electrolytes. Interestingly, the prepared Co(II) and Ni(II) complexes were employed as precursors for producing of Co_3O_4 and NiO nanoparticles, respectively. The produced nanostructures have been identified by XRD, HR-TEM, FT-IR and UV–Vis spectra. The produced nanoparticles revealed good photocatalytic activity for the degradation of methylene blue dye under UV illumination in presence of hydrogen peroxide. The percent of degradation was estimated to be 55.71% in 420.0 min and 90.43% in 360.0 min for Co_3O_4 and NiO, respectively. Moreover, the synthesized complexes, nano-sized Co_3O_4, and NiO products have been examined, employing modified Bauer- Kirby method, for antifungal (*Candida albicans* and *Aspergillus flavus*) and antibacterial (*Staphylococcus aureus* and *Escherichia coli*) activities.

1. Introduction

Triazole compounds especially 1,2,4-triazole derivatives have several interesting properties in various fields such as biological and industrial areas [1–4]. It was reported that 1,2,4-triazole Schiff base compounds can be used as antioxidant, antitumor and antimicrobial reagents [5–8]. This is based on that those compounds have significant role against bacteria and fungi, and this is probably owing to hetero atoms and/or azomethine linkage that these compounds contain. Recently, there is a great interest in preparation of new 1,2,4-triazole Schiff base complexes containing various metal ion centers. This is returning to that the biological efficiency enhances as a result of the ligand-metal linkage as illustrated by Overton's concept and chelation theory. Recently, metal ion complexes of Schiff bases proved their efficiency as cheap and inexpensive routes for producing of various metal oxide nanostructures [9,10]. Among those nano-sized metal oxides, Co_3O_4 and NiO still play a significant role due to their vast applications in electrode materials for supercapacitor [11], efficient anode in Li-ion battery [12], glycerol electrooxidation in alkaline medium [12], and photocatalytic degradation of dyes from aqueous solutions [13,14,15]. Notably, there are various methods for preparation of cobalt oxide and nickel oxide nanoparticles such as microwave-assisted template-free, hydrothermal, etc. [16–19]. However, these methods need long time and/or special equipment. Therefore, employing the coordination metal complexes as inexpensive precursors for the preparation of metal oxide nanostructures has been considered as one of the most convenient and practical routes [9]. Therefore, herein, we report on the preparation of novel Co(II) and Ni(II)-Schiff base complexes. The triazole Schiff base ligands were synthesized by condensation of 3-substitued-4-amino-5-hydrazino-1,2,4-triazole with dibenzoyl methane. The synthesized compounds were identified by means of Fourier Transform infrared

* Corresponding author.
E-mail addresses: m_y_nassar@yahoo.com, m_y_nassar@fsc.bu.eg.edu (M.Y. Nassar).

http://dx.doi.org/10.1016/j.molstruc.2017.04.118
0022-2860/

(FT-IR) spectrometer, Ultra Violet-Visible (UV–Vis) spectrometer, elemental analysis, conductivity, magnetic moment, and thermal analysis. Moreover, NiO and Co_3O_4 nanostructures were prepared using the corresponding Ni- and Co- Schiff base ligand complexes, respectively. The produced nanomaterials were characterized employing X-ray diffractometer (XRD), high resolution transmission electron microscope (HR-TEM), FT-IR, and UV–Vis spectra. The photocatalytic properties of the produced nano-sized products have been investigated using methylene blue dye aqueous solution under UV illumination in the presence of hydrogen peroxide. In addition biological activity of the produced nanostructures has been studied as well.

2. Experimental

2.1. Materials and reagents

Dibenzoylmethane, $NiCl_2 \cdot 6H_2O$ and $CoCl_2 \cdot 2H_2O$ were obtained from Aldrich chemical company. All solvents were of analytical reagent grade and used as received without further purification. The thiocarbohydrazide and 3-substituted-4-amino-5-hydrazino-1,2,4-triazoles were prepared as reported [20,21].

2.2. Synthesis of Schiff bases

The Schiff bases under study were prepared by condensation of 3-substituted-4-amino-5-hydrazino-1,2,4-triazole and dibenzoylmethane for 5 h, according to Scheme 1:

The produced yellow precipitate was filtered off, washed with cold ether and methanol then re-crystallized from ethanol and vacuum dried. The prepared Schiff bases are referred to as L1, L2 and L3 with 68.5, 77.5 and 75.5% yield in case of R=H, CH_3 and CH_2CH_3, respectively.

2.3. Synthesis of Co(II) and Ni(II) Schiff base complexes

The prepared Schiff base (one mmol): L1, L2 or L3, dissolved in 25 mL ethanol was added to an ethanolic solution of $NiCl_2 \cdot 6H_2O$ or $CoCl_2 \cdot 6H_2O$ (25 mL, one mmol), and refluxed for 5 h. After that, two mmol of sodium acetate trihydrate were added to the reaction blend and the reflux was continued for 5 h. Afterward, the complexes were collected by filtration, washed with ethanol, water, and ether and vacuum dried.

2.4. Synthesis of nanosized Co_3O_4 and NiO

Thermal decomposition of the as-synthesized Co(II) and Ni(II) - **L3** Schiff base complexes for 2 h at 650 °C, in an electric furnace, produced nano-sized Co_3O_4 and NiO, respectively.

2.5. Physical measurements

Functional groups of the triazole Schiff bases, their cobalt/nickel complexes, and cobalt/nickel oxides were investigated by collecting their FT-IR spectra using a Nicolet iSio FT-IR spectrophotometer in the 4000–400 cm^{-1} region in KBr disks. Electronic absorption spectra of the cobalt/nickel complexes were measured in *N,N*-dimethylformamide (DMF) and nujol oil using UV–Vis spectrophotometer (Jasco, model V-530). Employing tetramethyl silane (TMS) as an internal reference, the ^1H NMR spectra of the prepared triazole Schiff base compounds were carried out in a deuterated DMSO on a Bruker 300 MHz spectrometer at room temperature. CHN elemental analyses were obtained using Elementer Vario EL III Carlo Erba 1108 instrument. Molar conductivity measurements of the cobalt/nickel complexes were achieved using an YSI conductivity bridge with a cell having a cell constant = 1. Utilizing a Gouy balance, molar magnetic susceptibilities; χ_M, of the prepared

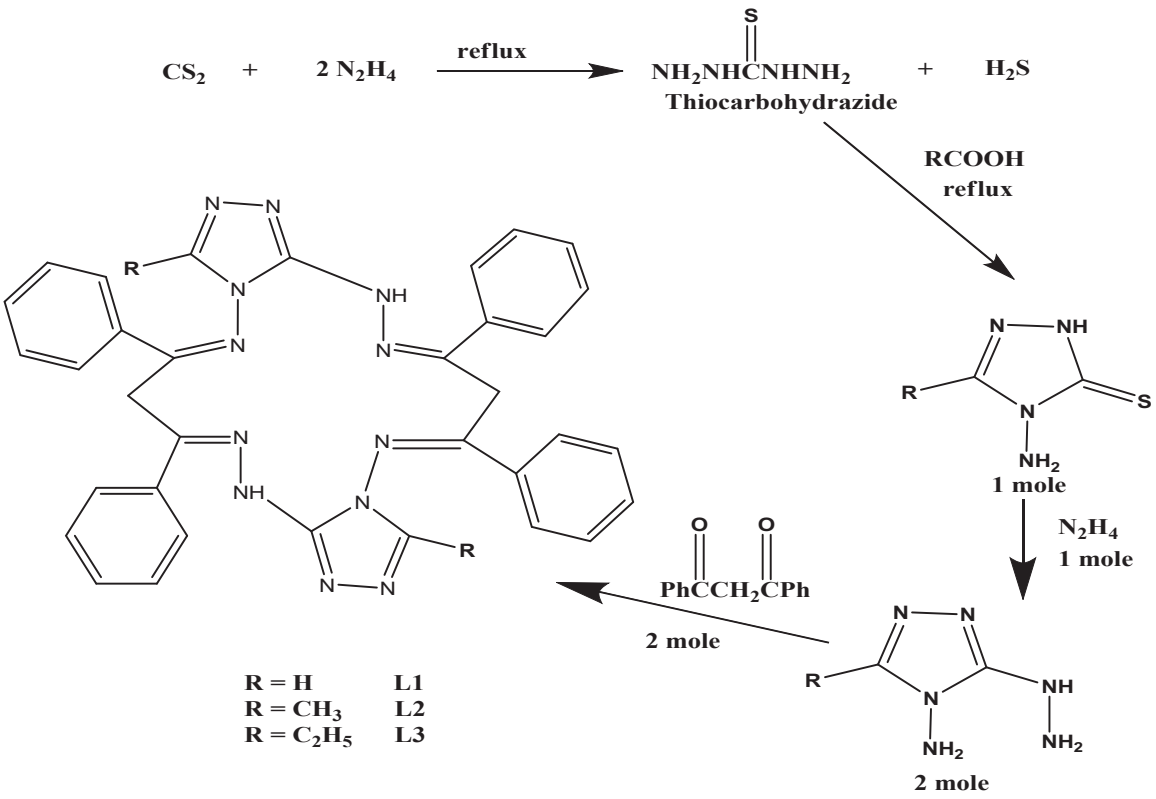

Scheme 1. Synthesis of Schiff bases.

complexes were estimated at room temperature. Consequently, the sample was packed in a Gouy tube of a known mass. Mercury (II) tetrathiocyanatocobaltate (II) [Hg {Co (SCN) 4}] was employed for the calibration of the Gouy tube. The diamagnetism correction was carried out using Pascal's constants. Thermal analyses of the prepared coalt/nickel complexes were collected using Shimadzu TA-60 WS thermal analyzer using N_2 atmosphere at heating rate of 10 °C min^{-1}. X-ray powder diffraction patterns (XRD) of cobalt/nickel oxides were measured on an 18 kW diffractometer (Bruker; model D8 Advance) with monochromated Cu Kα radiation (λ) 1.54178 Å. The HR-TEM images of cobalt/nickel oxides were obtained using a transmission electron microscope (JEOL; model 1200 EX) at an accelerator voltage of 220 kV.

2.6. Biological activity

The antimicrobial activities of the prepared triazole Schiff bases, their Co (II) and Ni (II) complexes, and as-fabricated cobalt/nickel oxide nanoparticles were estimated employing the modified Bauer-Kirby method [9]. It is worthy to mention that 100 μL of the pathogenic fungi/bacteria in 10 mL of fresh media were grown until they reached a count of 105 cells per mL for fungi or 108 cells per mL for bacteria. Then, 100 μL microbial suspensions were spread onto agar plates corresponding to the both pathogens in which they were maintained. Using a disc diffusion method, the isolated colonies of each organism were examined for susceptibility. After that a filter paper disc impregnated with the tested compounds was placed on agar where plates with fungi (*Candida albicans* and *Aspergillus flavus*) were incubated for 24–48 h at 25–27 °C. And, the plates with gram positive bacteria (*Staphylococcus aureus*)/gram negative bacteria (*Escherichia coli*) were kept for 24–48 h at 35–37 °C. The inhibition zone diameters were then determined in millimeters.

2.7. Photocatalytic activity measurements

The Photocatalytic activities of the metal oxides produced using L3-Ni or -Co complexes were examined by studying the degradation of methylene blue dye. This experiment was carried out by stirring 0.1 g of the prepared cobalt/nickel oxide photocatalyst in 50 mL of 10 mg/L aqueous dye solution. This stirring was performed in dark for 2 h to attain an adsorption-desorption equilibrium. Then, 2 mL of 0.2 M hydrogen peroxide solution was added, the UV light (at 365 nm) was turned on, and stirring of the suspension was continued. It is worthy to mention that the degradation study was performed in a Pyrex beaker under the UV illumination using a 250 W xenon arc lamp (Thoshiba, SHLS-002) (λ = 365 nm). At a pre-defined intervals, aliquots were taken out of the beaker, the cobalt/nickel oxide catalyst was separated by centrifugation, and the absorption of remaining solution is measured at 664 nm (λ_{max} for methylene blue dye) employing a UV–Vis spectrophotometer.

3. Results and discussion

3.1. Preparation and characterization of L1, L2 and L3 triazole Schiff base ligands

Three novel Schiff bases have been prepared through the condensation reaction of 3-R-4-amino-5-hydrazino-1,2,4-triazole (R=H, CH_3 or C_2H_5) and dibenzoylmethane in methanol at a molar ratio of 1:1. This reaction was performed in the presence of a few drops of concentrated H_2SO_4 at refluxing temperature. The prepared Schiff bases were elucidated utilizing CHN elemental analysis, m.p, FT-IR, and ^{1}H NMR. The obtained C, H, and N % values are consistent with the suggested molecular formulas (Theoretical values) (*c.f.* Table 1).

3.1.1. IR spectra of L1, L2 and L3 triazole Schiff bases

The FT-IR spectra of the prepared triazole Schiff base compounds revealed various peaks (*c.f.* Fig. 1 and Table 2). A broad band with medium intensity was observed in the range 3500–3470 cm^{-1} attributing to NH stretching vibration of the triazole ring and OH stretching vibration of the adsorbed water molecules. Moreover, a medium band appeared in the range 1628–1620 cm^{-1} can assigned to C=N stretching vibration, and bending vibration of the adsorbed water molecules [10]. Various absorption bands were observed in the region 1570-1400 cm^{-1} attributing to C=C aromatic stretching vibrations whereas peaks in the region of 785–745 cm^{-1} assigning to C–H out of plane aromatic ring bending vibration [22].

3.1.2. ^{1}H NMR spectra of L1, L2 and L3 triazole Schiff bases

The ^{1}H NMR spectra (*c.f.* Table 2) (in DMSO-d_6) of the prepared triazole Schiff base compounds exhibited signals at ca.: 11.20 (s, 2H, NH) (L1 and L3), 11.40 (s, 2H, NH) (L2), 7.20–8.40 (m, 20H, Ar–H), 4.85 (s, 4H, aliphatic CH_2), 6.33 (s, 2H, H-Triazole- L1), 2.40 (s, 6H, CH3-Triazole- L2), 1.19 (t, 6H, CH_3-Triazole- L3) and 2.65 (q, 4H, CH_2-Triazole-L3) [23]. The NH disappearance in ^{1}H NMR spectrum (DMSO-d_6-D_2O) indicating the presence of NH in the prepared compounds.

3.2. Preparation and characterization of Co(II) and Ni(II) triazole Schiff base complexes

Solid Co(II) and Ni(II) complexes of triazole Schiff base have been prepared via refluxing the prepared Schiff bases with $CoCl_2 \cdot 6H_2O$ or $NiCl_2 \cdot 6H_2O$ in ethanol at a molar ratio of 1:1 ratio in the presence of sodium acetate trihydrate. All the prepared Co(II) and Ni(II) complexes are stable at room temperature, and soluble in DMSO and DMF. The prepared complexes have been identified using various techniques such as CHN elemental analyses (*c.f.* Table 1), molar conductivity (*c.f.* Table 5), FT-IR spectra, magnetic moments, thermal analysis, and UV–Vis spectra. The Practically obtained elemental analysis values are in accordance with the suggested molecular formulas (Theoretical values). Additionally,

Table 1
Physical properties and micro-elemental analyses of the prepared Schiff bases (L1, L2, and L3) and their Co(II) and Ni(II) metal complexes.

Compound	m.p	Molecular formula	Analyzed element % calculated found		
			C	H	N
L1	92–93	$C_{34}H_{28}N_{12}$	67.54	4.67	27.80
			66.89	4.40	28.21
L2	112–113	$C_{36}H_{32}N_{12}$	68.34	5.10	26.56
			68.67	5.33	26.00
L3	130–131	$C_{38}H_{36}N_{12}$	69.07	5.49	25.44
			69.34	5.02	25.64
Co-L1	–	$C_{34}H_{32}Cl_2CoN_{12}O_2$	53.00	4.19	21.81
			53.00	3.99	21.79
Co-L2	–	$C_{34}H_{32}Cl_2CoN_{12}O_2$	54.14	4.54	21.05
			54.60	4.29	21.56
Co-L3	–	$C_{38}H_{42}Cl_2CoN_{12}O_3$	51.83	4.32	21.34
			51.90	4.40	21.41
Ni-L1	–	$C_{34}H_{32}Cl_2N_{12}NiO_2$	53.01	4.19	21.82
			53.23	4.45	21.45
Ni-L2	–	$C_{36}H_{36}Cl_2N_{12}NiO_2$	54.16	4.55	21.05
			54.09	4.86	21.03
Ni-L3	–	$C_{38}H_{42}Cl_2N_{12}NiO_3$	51.99	5.34	21.37
			51.72	5.49	22.01

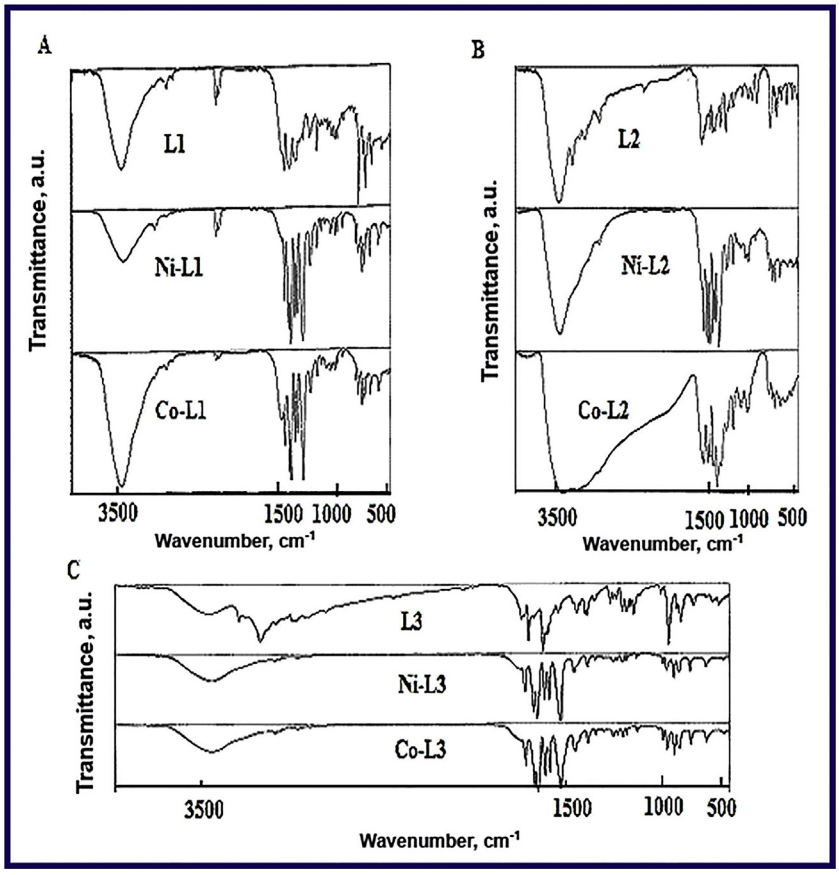

Fig. 1. FT-IR spectra of (A) L1- metal complexes (B) L2- metal complexes (C) L3- metal complexes.

Table 2
^{1}H NMR and FT-IR peaks of the prepared Schiff bases.

Compound	^{1}H NMR (δ, ppm)	FT- IR (cm^{-1})
L1	11.2 (s, 2H, NH)	3470 (NH– stretching)
	7.2–8.4 (m, 20H, Ar–H)	1625 (C=N- stretching)
	4.8 (s, 4H, CH_2 aliphatic)	1575 (C=C- aromatic stretching)
	6.3 (s, 2H, H-Triazole)	1492 (NH bending vibration)
		743 (C–H, aromatic pending)
L2	11.40 (s, 2H, NH)	3480 (NH– stretching)
	7.2–8.4 (m, 20H, Ar–H)	1623 (C=N- stretching)
	4.8 (s, 4H, CH_2 aliphatic)	1570 (C=C- aromatic stretching)
	2.40 (s, 6H, CH_3-Triazole)	1485 (NH bending vibration)
		755 (C–H, aromatic pending)
L3	11.20 (s, 2H, NH)	3500 (NH– stretching)
	7.2–8.4 (m, 20H, Ar–H)	1620 (C=N- stretching)
	4.8 (s, 4H, CH_2 aliphatic)	1550 (C=C- aromatic stretching)
	1.19 (t, 6H, CH_3-Triazole)	1490 (NH bending vibration)
	2.65 (q, 4H, CH_2-triazole)	760 (C–H, aromatic pending)

the obtained molar conductivity measurements at concentration of 10^{-3} M in DMF indicate the non-electrolytic nature of the prepared complexes.

3.2.1. IR spectra of Co(II) and Ni(II) triazole Schiff base complexes

The FT-IR spectra of the all prepared Schiff base complexes revealed a medium and broad band in the range 3500–3470 cm^{-1} (*c.f.* Fig. 1 and Table 3) attributing to NH stretching vibration of the triazole ring. And, this indicates that NH is not coordinated to the metal ion. The spectra also revealed a medium to high intensity band in the range 1628–1620 cm^{-1} which can be attributed to C=N stretching vibration which decreased by 20–25 cm^{-1} [10]. This supports the triazole Schiff base coordination to cobalt/nickel through the C=N nitrogen. Furthermore, this is also supported by the existence of a medium intensity band in the region of 525–523 cm^{-1} due to Co/Ni–N stretching vibration [23].

3.2.2. Electronic spectra of Co(II) and Ni(II) triazole Schiff base complexes

The electronic absorption spectra of the prepared Co(II) and Ni(II) complexes (in dry DMF and Nujol mull) are tabulated in Table 4. All the obtained data supported that all the geometries of the synthesized complexes are octahedral in case of Co(II) complexes and distorted octahedral in case of Ni(II) complexes [9]. Consequently, the chemical structures of the prepared complexes in solid state can be represented as shown in Scheme 2.

3.2.3. Magnetic studies and conductivity measurements of Co(II) and Ni(II) triazole Schiff base complexes

The obtained magnetic moments at room temperature are tabulated in Table 5. The magnetic measurements for Co(II) and Ni(II) complexes are 4.35–4.98 B.M. and 2.79–3.54 B.M., respectively, and these are in good agreement with their octahedral environment [9]. The magnetic moments of Co(II) complexes with ligands L1, L2 and L3 are 4.88, 4.35 and 4.50 BM, respectively which are higher than the spin-only value 3.87 BM. This indicates that orbital contribution to the magnetic moment is not significant and can be neglected compared to that of the spin-only value.

It is well-known that for an electron to have an orbital angular momentum, it must be possible that the orbital that it occupies can be transformed to into an exactly equivalent and degenerate orbital by rotation.

Table 3
FT-IR band positions (cm^{-1}) of the prepared Schiff bases complexes.

Compound	Co(II) complexes	Ni(II) complexes
Complexes of L1	3500 (NH– stretching, OH– stretching)	3495 (NH– stretching, OH– stretching)
	1605 (C=N- stretching, OH bending)	1602 (C=N- stretching, OH bending)
	1575 (C=C- aromatic stretching)	1578 (C=C- aromatic stretching)
	785 (C–H– aromatic pending)	760 (C–H, aromatic pending)
	528 (Co–N– stretching)	525 (Ni–N– stretching)
Complexes of L2	3480 (NH– stretching, OH– stretching))	3490 (NH– stretching, OH– stretching)
	1600 (C=N- stretching, OH bending)	1600 (C=N- stretching, OH bending)
	1580 (C=C- aromatic stretching)	1579 (C=C- aromatic stretching)
	785 (C–H, aromatic pending)	780 (C–H, aromatic pending)
	518 (Co–N– stretching)	520 (Ni–N– stretching)
Complexes of L3	3495 (NH– stretching, OH– stretching))	3485 (NH– stretching, OH– stretching)
	1594 (C=N- stretching, OH bending)	1600 (C=N- stretching, OH Bending)
	1585 (C=C- aromatic stretching)	1575 (C=C- aromatic stretching)
	790 (C–H, aromatic pending)	785 (C–H, aromatic pending)
	510 (Co–N– stretching)	515 (Ni–N– stretching)

Table 4
Electronic absorption spectral data of solid Co(II) and Ni(II)- L1, L2 and L3 Schiff bases complexes.

Complex	CT band		d→d bands		
	Nujol mull	DMF	Nujol mull	DMF	Assignment
Co-L1	28359	28571	8270	8264	$^4\mathbf{T_{1g}(F)} \rightarrow {}^4\mathbf{T_{2g}(F)}$
Co-L2	25421	28328	8240	8230	$^4\mathbf{T_{1g}(F)} \rightarrow {}^4\mathbf{T_{2g}(F)}$
Co-L3	28245	28127	8245	8244	$^4\mathbf{T_{1g}(F)} \rightarrow {}^4\mathbf{T_{2g}(F)}$
Ni-L1	–	–	28237	26322	$^3\mathbf{A_{2g}} \rightarrow {}^3\mathbf{T_{1g}(P)}$
			14960	15223	$^3\mathbf{A_{2g}} \rightarrow {}^3\mathbf{T_{1g}(F)}$
			11789	11522	$^3\mathbf{B_{1g}} \rightarrow {}^3\mathbf{B_{2g}}$
			10157	10456	$^3\mathbf{B_{1g}} \rightarrow {}^3\mathbf{E_g}$
Ni-L2	–	–	25157	28754	$^3\mathbf{A_{2g}} \rightarrow {}^3\mathbf{T_{1g}(P)}$
			14714	15673	$^3\mathbf{A_{2g}} \rightarrow {}^3\mathbf{T_{1g}(F)}$
			11884	11820	$^3\mathbf{B_{1g}} \rightarrow {}^3\mathbf{B_{2g}}$
			10352	10387	$^3\mathbf{B_{1g}} \rightarrow {}^3\mathbf{E_g}$
Ni-L3	–	–	24384	27450	$^3\mathbf{A_{2g}} \rightarrow {}^3\mathbf{T_{1g}(P)}$
			13769	14887	$^3\mathbf{A_{2g}} \rightarrow {}^3\mathbf{T_{1g}(F)}$
			11540	11940	$^3\mathbf{B_{1g}} \rightarrow {}^3\mathbf{B_{2g}}$
			10380	10065	$^3\mathbf{B_{1g}} \rightarrow {}^3\mathbf{E_g}$

In an octahedral complex, the degenerate t_{2g} orbitals (d_{xz}, d_{yz}, d_{xy}) can be inter-converted by 90° rotation. However the e_g orbitals (d_{z2}, d_{x2-y2}) cannot be inter-converted by rotation about any axis because of their different shapes, thus electrons in the e_g set cannot contribute to orbital angular momentum.

On the other hand, electrons in t_{2g} orbitals will not always contribute into the orbital angular momentum. The following configurations only have orbital contribution to magnetic moment: $^1t_{2g}$, $^2t_{2g}$, $^4t_{2g}$ and $^5t_{2g}$, but $^3t_{2g}$ and $^6t_{2g}$ configurations do not have orbital contribution to magnetic moment.

The Co(II) ion (d^7) has either $^5t_{2g}^2e_g$ configuration with ground term $^4T_{1g}$ or $^6t_{2g}^1e_g$ configuration with ground term ^2E_g. Only, the first case has orbital contribution to magnetic moments. This is agreement with the spectroscopic data presented in Table 5 with ground term $^4T_{1g}$ (F).

For the Ni (II) (d^8) complexes, the electronic configurations are $^6t_{2g}^2e_g$ with ground term $^3A_{2g}$, which have no orbital contribution to the magnetic moments. The values of magnetic moments for these two complexes are 2.79–3.54 BM (*c.f.*Table 5) which is slightly higher than the spin only values; 2.83.

For A_2 terms, the magnetic moment is given by David

$$\mu_{eff} = \mu_{spin\ \ only}[1 - (\alpha\lambda/10\ \ Dq)]$$

where $\alpha = 4$ for an A_2 term. The spin-orbital coupling constant λ has a positive sign for d shells less than half- filled and is negative for d shells more than half- filled. Thus, the d^8 (Ni^{+2}) ion have λ negative and hence their $\mu_{eff} > \mu_{spin\ only}$.

The molar conductivities of the solid Co(II) and Ni(II) complexes in DMF are tabulated in Table 5. The molar conductivity values fall in the range of 24–28 Ω^{-1} cm^2 mol^{-1} indicating the non-electrolyte nature of the prepared complexes [9].

Table 5
Magnetic studies and Conductivity measurements of solid Co(II) and Ni(II)- L1, L2 and L3 Schiff bases complexes.

Compound	Magnetic moment (B.M)	Molar conductivity $\Omega^{-1}cm^2mol^{-1}s$
Co-L1	4.88	28.9
Co-L2	4.35	26.8
Co-L3	4.50	27.8
Ni-L1	3.54	24.7
Ni-L2	3.28	28.6
Ni-L3	2.79	28.1

3.2.4. Thermal analysis of the prepared Co(II) and Ni(II) Schiff base complexes

TG, DTG, and DTA curves (***c.f.*** Fig. 2) for Co-**L3** Schiff base complex exhibited four endothermic decomposition steps. The first stage appeared in the temperature range of 33–270 °C corresponding to loss of two adsorbed water molecules (4.57%, found 3.95%). The second step appeared in the temperature range of 270–330 °C which can be attributed to loss of two HCl molecules with a weight loss of 9.2% (calc. 9.14%). The last two weight losses occurred in the temperature range of 330–430 and 430–660 °C can be assigned to decomposition of the organic moiety and remaining water molecule with a total weight loss of 75.6% (calc. 75.59%). And, this last weight loss step generated Co_3O_4 +1C residue with 11.25% (calc. 10.70%).

On the other hand, Ni-**L3** Schiff base complex decomposed similarly in four endothermic decomposition steps as shown in TG and DTG curves (Fig. 2). The first decomposition step occurred in the temperature range of 50–250 °C attributing to two adsorbed water molecules loss (4.58%, found 3.9%). The second decomposition stage revealed in the temperature range of 250–330 °C which can be assigned to two HCl molecules loss with a weight loss of 9.3% (calc. 9.15%). The last two weight losses appeared in the temperature range of 300–400 and 400–650 °C can be returned to the decomposition of organic content and the remaining water molecule with a total mass loss of 76.0% (calc. 75.34%). Moreover, the decomposition of the organic ligand in the last two steps produced NiO +1C residue with 10.8% (calc. 10.93%).

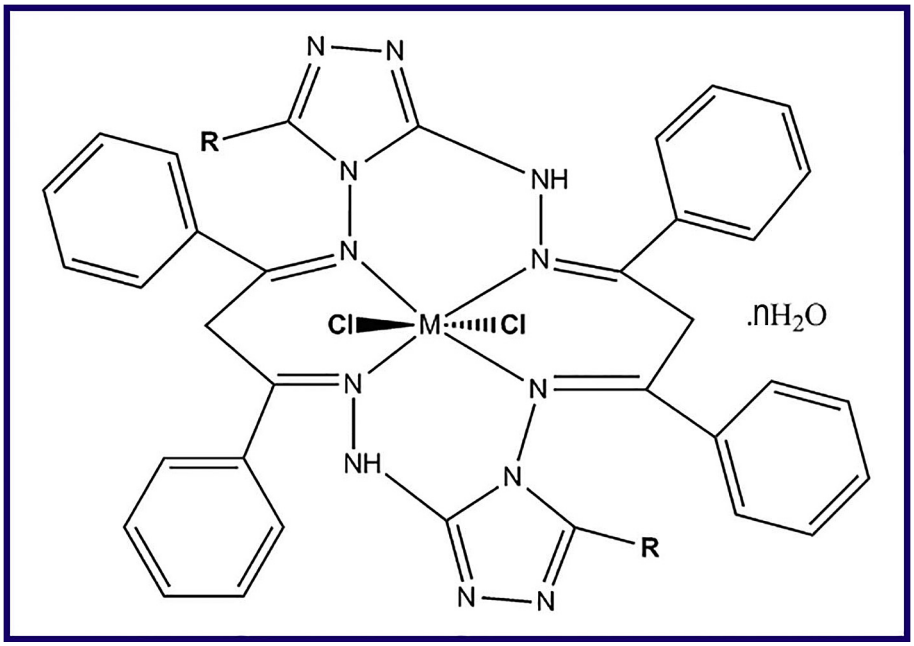

Scheme 2. Proposed chemical structures of Schiff base complexes.

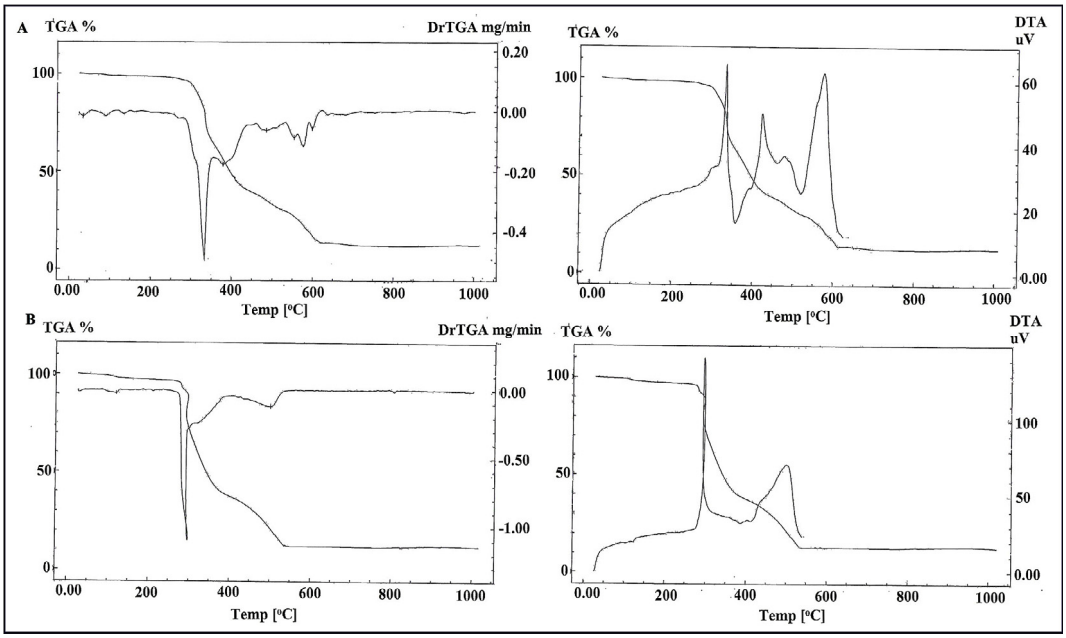

Fig. 2. TGA, DTG, and DTA of (A) Co- L3 (B) Ni- L3.

3.3. Synthesis and characterization of Co_3O_4 and NiO nanoparticles

The prepared solid complexes Co(II)-L3 and Ni(II)-L3 were thermally decomposed at 650 °C to give the corresponding cobalt and nickel oxides; The generated cobalt/nickel oxides were elucidated utilizing various tools such as XRD, HR-TEM, FT-IR, and UV–Vis spectra. Therefore, cobalt/nickel oxide nanoparticles could be synthesized employing a simple and fast chemical method without using toxic solvents and expensive or complicated equipment.

3.3.1. XRD and HR-TEM analysis of Co_3O_4 and NiO

Fig. 3(A and B) shows the XRD patterns of the produced cobalt oxide and nickel oxide nanoparticles, respectively. It is clear from XRD patterns that all the reflections can be indexed well to pure Co_3O_4 and NiO nanoparticles, respectively. We have not observed any reflection peaks due to impurities proving the high purity of the prepared oxides. Moreover, their relative intensities can be perfectly indexed into **(i)** The cubic phase of Co_3O_4 with cell constants: a = b = c = 8.085 Å (space group Fd-3m, JCPDS card 78–1970); these data are consistent with the reported data

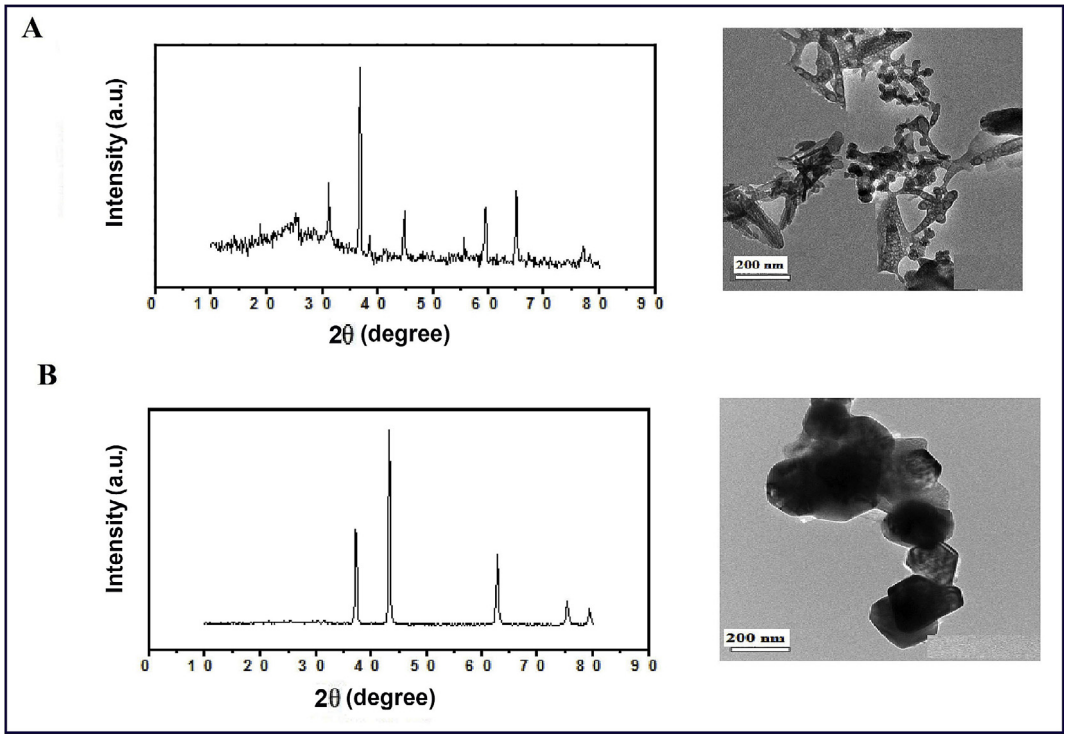

Fig. 3. XRD pattern and HR-TEM image of (A) Co_3O_4 and (B) NiO products.

[24–28]. **(ii)** The Rhombohedral phase of NiO with cell constants: a = b = 2.955 Å, and c = 7.228 Å (space group R-3m, JCPDS card 44–1159); these data are in good accordance with the data reported by S. Z. Khan et al. [29]. The following Debye–Scherrer equation was utilized to calculate the average crystal size of the cobalt/nickel oxide nanoparticles.

$$D = 0.9\lambda/\beta\cos\theta_B$$

where, λ, β, Θ_B are the X-ray wavelength, the full width at half maximum (FWHM) of the diffraction peak and the Bragg diffraction angle, respectively. The determined crystallite sizes of Co_3O_4 and NiO, from XRD data, are estimated to be 43.37 and 49.68 nm, respectively. On the other hand, the HR-TEM image Co_3O_4 (Fig. 3(A)) revealed that this product is composed of spherical, rood and irregular shaped aggregates with average particle size of 35.21 nm. Whereas the HR-TEM image Co_3O_4 (Fig. 3(B)) exhibited that NiO product is composed spherical and irregular shaped aggregates with average particle size of 65.34 nm.

3.3.2. FT-IR of Co_3O_4 and NiO nanoparticles

The FT-IR spectra of Co_3O_4 (Fig. 4) show two strong absorption bands at 666 and 573 cm^{-1} which confirm the spinel structure of Co_3O_4 product. The first peak is attributed to the stretching vibration mode of MO in which M is Co^{2+} and is tetrahedrally coordinated, and the second peak can be assigned to M–O in which M is Co^{3+} and is octahedrally coordinated [9,30,31].Whereas, the FT-IR spectra of NiO (Fig. 4) show several significant absorption peaks. The broad absorption band at 471 cm^{-1} is assigned to Ni–O stretching vibration mode; the broadness of the absorption band indicates that the NiO powders are nanocrystals. The broad absorption band centered at 3442 cm^{-1} is attributable to the band O–H stretching vibrations of the adsorbed water molecules [32–38]. The weak band appeared at ca. 1630 cm^{-1} attributed to OH bending vibrations of the adsorbed water molecules on the surface of the produced oxides. These results are consistent with the published data [32–38].

3.3.3. Optical properties of Co_3O_4 and NiO

In order to investigate the semiconducting characteristics of the prepared coalt/nickel oxide nanoparticles, UV–Vis absorption spectra were performed and depicted as shown in Fig. 4. The optical band energy gap E_g was determined employing the following equation:

$$(\alpha h\upsilon)^n = K(h\upsilon - E_g)$$

where K is a constant, α is the absorption coefficient, E_g is the optical band energy gap. And, n equals either 2 for a direct allowed transition or 1/2 for an indirect allowed transition. In case of the prepared cobalt/nickel oxides, hυ (eV) is plotted against $(\alpha h\upsilon)^2$, as shown in Fig. 4. The extrapolation of each graph to zero value of $(\alpha h\upsilon)^2$ results in the direct optical band gap (E_g) which is determined to be 3.90 and 3.00 eV for Co_3O_4 and NiO nanoparticles, respectively. These values exhibited that the as-prepared Co_3O_4 and NiO nanoparticles products are semiconductors. These values are consistent with the reported data [9].

4. Biological activities

The in-vitro biological activity of the prepared Schiff base compounds:L1, L2 and L3, their Co (II) and Ni (II) complexes, and as-synthesized cobalt/nickel oxides were examined using bacteria, *Staphylococcus aureus* and *Escherichia coli* and fungi, *Candida albicans* and *Aspergillus flavus*. In antimicrobial studies ampicillin was selected as antibacterial agent whereas, amphotericin b was selected as antifungal agent and the two worked together as positive control. Negative control of antimicrobial studies was performed through filter disc impregnated with 10 μL of solvent (DMSO). The investigated compounds diffuse from the disc into the

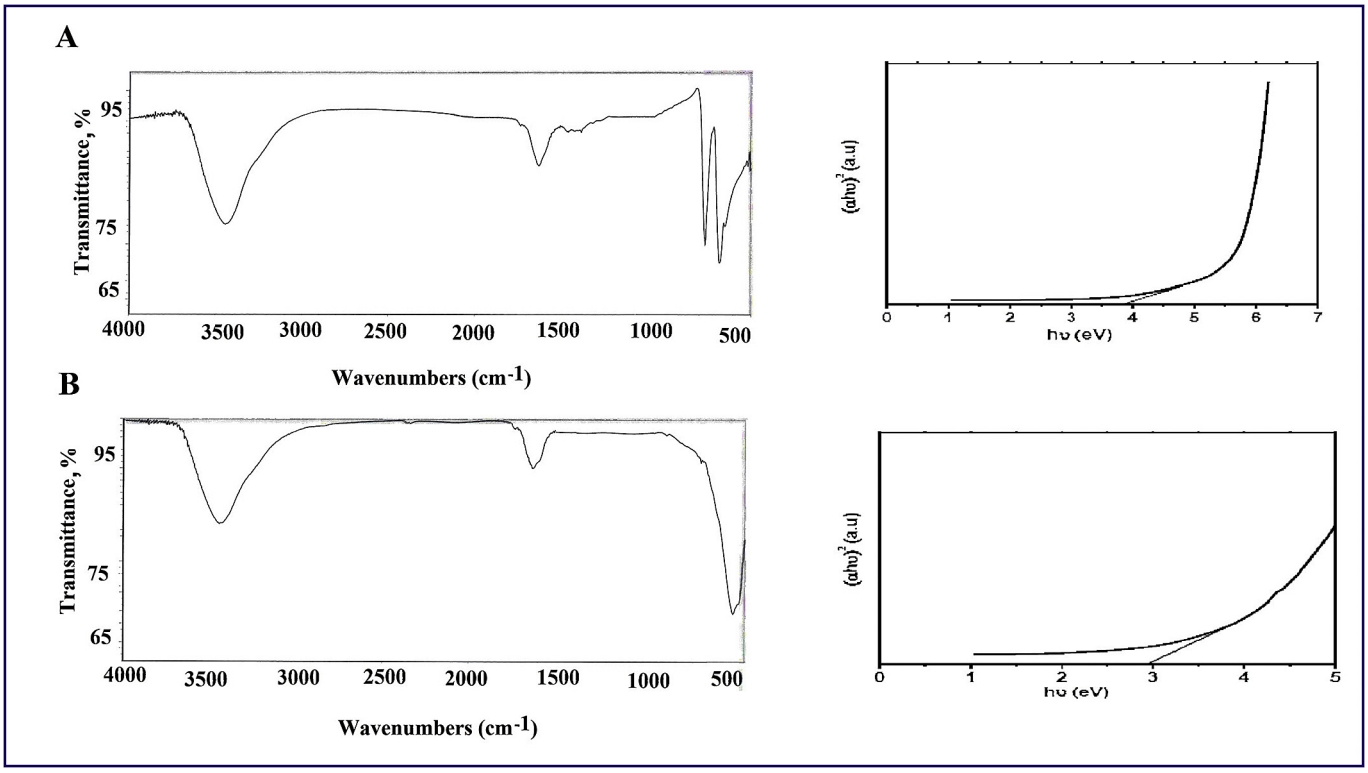

Fig. 4. FT-IR spectrum and optical energy gap of (A) Co_3O_4 and (B) NiO products.

agar; only around the disc during the time of incubation. When the organism is exposed to the compounds, it will not grow in an area around the disc called "zone of inhibition", which measured and presented in Table 6. The Schiff base L3 compound revealed very strong activity against all pathogens (both bacteria and fungi). All examined compounds exhibited moderate activity against both pathogenic bacteria strains and poor antifungal activity. All Co (II) and Ni (II) complexes revealed no activity on *A. flavus* fungi and moderate activity on *C. albicans* fungi. All the as-synthesized oxides showed no activity against both pathogenic bacteria strains and antifungal.

5. Photocatalytic activity study of Co_3O_4 and NiO

Photocatalytic activity of the as-prepared oxides; Co_3O_4 and NiO, produced Co-L3 and Ni-L3 complexes, respectively, has been studied using methylene blue dye under ultraviolet radiation in presence of hydrogen peroxide via photo Fenton reaction [9]. UV–Vis spectra of the remaining dye during the photo-degradation have been measured and depicted in Fig. 5 (**A and B**). It was found that the maximum percent of degradation was found to be 55.71% after 420 min, and 90.43% after 360 min for Co_3O_4 and NiO, respectively, which is considered a very high percent compared with others in literature [9]. Many experiments have been carried out to study the degradation process under different conditions: in the presence of UV only, (Cobalt/Nickel Catalyst + UV) and (UV + Cobalt/Nickel Catalyst + H_2O_2). Photo-degradation reaction mechanism in the presence of UV only, (Cobalt/Nickel Catalyst + UV) and (UV + Cobalt/Nickel Catalyst + H_2O_2) has been presented in Scheme 3.

It is worthy to mention that UV radiation interacts with methylene blue dye molecules, and this interaction results in producing of excited dye molecules. Then the excited dye molecules react with oxygen to give positive radical of dye ($MB^{+\cdot}$) and negative radical of oxygen ($O_2^{-\cdot}$). Afterward, the negative radical interacts with H^+ liberated from water to produce super oxide radicals ($OOH^{\cdot}$) which known by their high power for the degradation of the dye molecule. In case of UV radiation + cobalt/nickel oxide catalyst, the interaction between cobalt/nickel oxide and ultraviolet radiation generates holes (h^+) and electrons (e^-) on the surface of the oxide catalyst. The generated electrons will then react with oxygen to produce negative oxygen anion radical ($O_2^{-\cdot}$) interacting with water molecules producing super oxide radical ($OOH^{\cdot}$). Whereas, holes accumulated on oxide surface will react with water and hydroxide anion to produce hydroxide radical ($OH^{\cdot}$). Both hydroxide and superoxide radicals will effectively increase the rate of dye molecules degradation. Moreover, addition of hydrogen peroxide to the catalyst under UV light produces large number of hydroxide radical ($OH^{\cdot}$) along with superoxide radicals ($OOH^{\cdot}$) which results in enhancement in photocatalytic degradation rate of the methylene blue dye molecules.

Table 6
The antimicrobial activity (in vitro) of the prepared Schiff bases (**L1**, **L2** and **L3**) and their Co(II) and Ni(II) complexes.

Compound	Bacteria		Fungi	
	E. coli (G^-)	*S. aureus* (G^+)	*A. flavus*	*C. albicans*
L1	11	11	9	9
L2	11	11	9	9
L3	30	31	26	9
Co-L1	10	10	9	11
Co-L2	14	12	0.0	13
Co-L3	11	11	9	12
Ni-L1	9	10	0.0	9
Ni-L2	11	11	0.0	13
Ni-L3	10	9	9	9
Co_3O_4	0	0	0.0	0
NiO	0	0	0.0	0

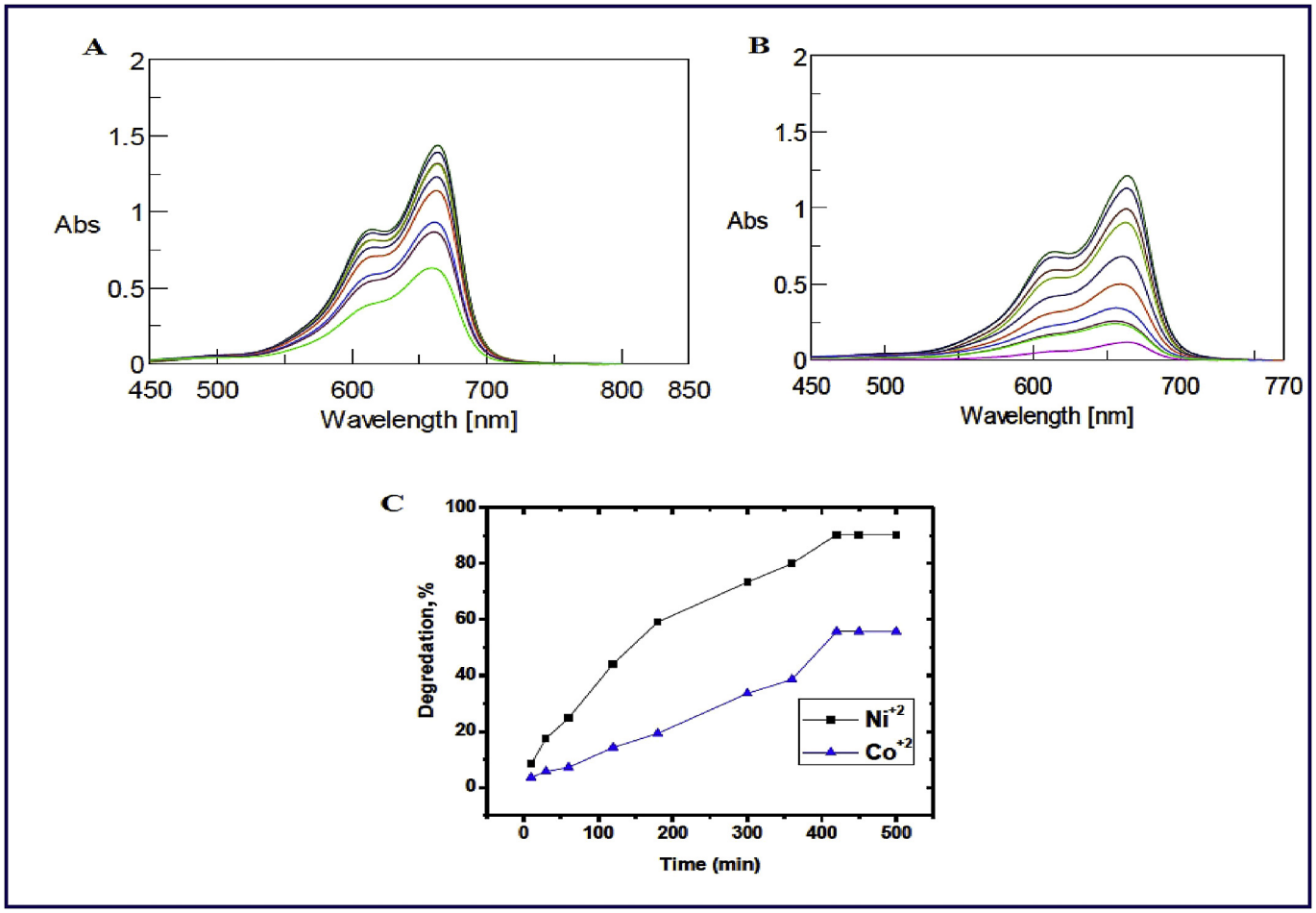

Fig. 5. Photocatalytic degradation of MB dye using (A) Co_3O_4, (B) NiO, and (C) % degradation versus time.

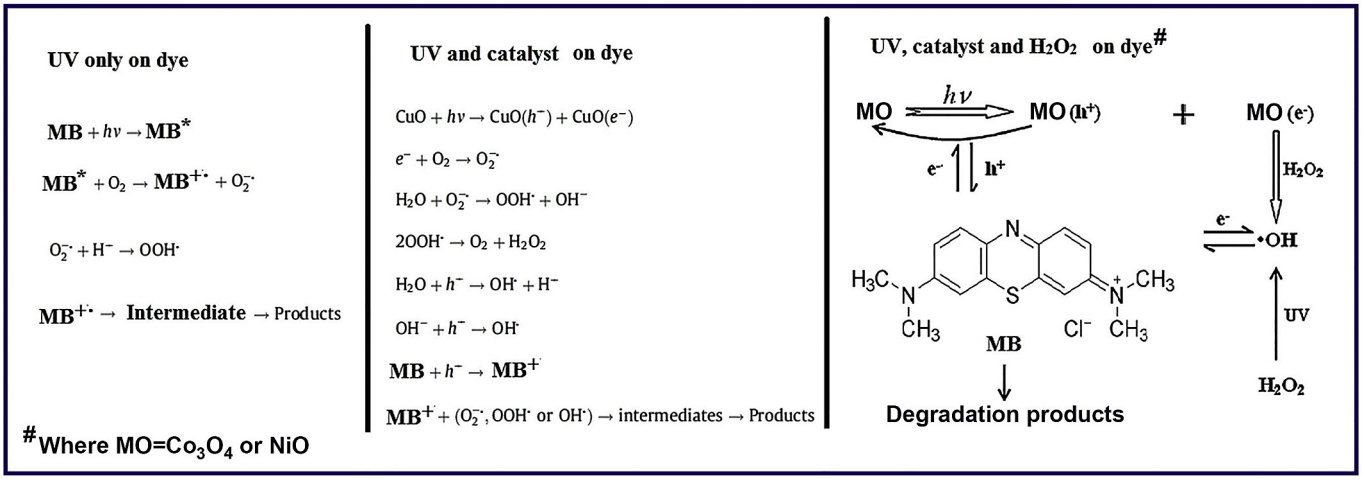

Scheme 3. Proposed reactions for the photodegradation of MB dye in the presence of UV only, (Catalyst + UV) and (UV + Catalyst + H_2O_2).

6. Conclusion

In summary, six novel Co(II) and Ni(II)-Schiff base complexes were successfully prepared. The Schiff bases were obtained by condensation of 3-R-4-amino-5-hydrazino-1,2,4-triazole with dibenzoyl-methane [R═H, CH_3, and CH_2CH_3 namely L1, L2, and L3, respectively]. The prepared complexes have been identified using elemental analysis, magnetic moment, UV–Vis spectra, FT-IR spectra, conductivity, and thermal analysis. The prepared cobalt/nickel complexes are non-electrolytes. Cobalt oxide and nickel oxide nanostructures were successfully fabricated through thermal decomposition of the prepared cobalt/nickel complexes. The produced nanostructures were identified by XRD, HR-TEM, FR-IR, and UV–Vis spectra. The produced oxide nanoparticles showed high

photocatalytic activity for the degradation of methylene blue dye in the presence of hydrogen peroxide under UV illumination. The percentage of degradation of methylene blue dye was found to be 55.71% after 420 min and 90.43% after 360 min for Co_3O_4 and NiO, respectively. The produced cobalt/nickel oxides exhibited moderate activity against both pathogenic bacteria strains and poor anti-fungal activity.

References

[1] R. Shukla, T.P. Mohan, B. Vishalakshi, D. Chopra, J. Mol. Struct. 1134 (2017) 426–434.
[2] A.E.-B.A.G. Ghattas, H.M. Moustafa, E.A.A. Hassanein, B.R.M. Hussein, Arab. J. Chem. 9 (2016) 1654–1659.
[3] Z. Song, Y. Liu, Z. Dai, W. Liu, K. Zhao, T. Zhang, Y. Hu, X. Zhang, Y. Dai, Bioorg. Med. Chem. 24 (2016) 4723–4730.
[4] N. Kulabas, E. Tatar, O. Bingol Ozakpinar, D. Ozsavci, C. Pannecouque, E. De Clercq, I. Kucukguzel, Eur. J. Med. Chem. 121 (2016) 58–70.
[5] K. Wajda-Hermanowicz, D. Pieniążczak, R. Wróbel, A. Zatajska, Z. Ciunik, S. Berski, J. Mol. Struct. 1114 (2016) 108–122.
[6] R. Alphonse, A. Varghese, L. George, J. Mol. Struct. 1113 (2016) 60–69.
[7] B.N. Prasanna Kumar, K.N. Mohana, L. Mallesha, J. Fluor. Chem. 156 (2013) 15–20.
[8] H. Khanmohammadi, M. Erfantalab, G. Azimi, Spectrochim. Acta. A. 105 (2013) 338–343.
[9] H.M. Aly, M.E. Moustafa, M.Y. Nassar, E.A. Abdelrahman, J. Mol. Struct. 1086 (2015) 223–231.
[10] M.Y. Nassar, A.S. Attia, K.A. Alfallous, M.F. El-Shahat, Inorg. Chim. Acta 405 (2013) 362–367.
[11] X.W. Wang, D.L. Zheng, P.Z. Yang, X.E. Wang, Q.Q. Zhu, P.F. Ma, L.Y. Sun, Chem. Phys. Lett. 667 (2017) 260–266.
[12] Y. Zhang, Q. Zhuo, X. Lv, Y. Ma, J. Zhong, X. Sun, Electrochim. Acta. 178((2015) 590–596.
[13] Y. Su, Q. Xu, Q. Zhong, C. Zhang, S. Shi, C. Xu, Mater. Res. Bull. 64 (2015) 301–305.
[14] T. Linda, S. Muthupoongodi, X.S. Shajan, S. Balakumar, Int. J. Light. Elec. Optic. 127 (2016) 8287–8293.
[15] S.A. Singh, B. Vemparala, G. Madras, J. Environ. Chem. Eng. 3 (2015) 2684–2696.
[16] Y. Li, K. Keith, N. Chopra, J. Alloy. Compd. 703 (2017) 414–423.
[17] H. Sun, W. Zhu, Appl. Sur. Sci. 399 (2017) 298–304.
[18] H. Sun, W. Zhu, Powd. Technol. 311 (2017) 132–136.
[19] S. Liu, W. Zeng, T. Chen, Phys. E. Low. Dimens. Syst. Nanostruct. 1086 (2015) 223–231.
[20] G.B. Bagihalli, S.A. Patil, J. Coord. Chem. 62 (2009) 1690–1700.
[21] B. Shivarama Holla, B. Veerendra, M.K. Shivananda, B. Poojary, Eur. J. Med. Chem. 38 (2003) 759–767.
[22] A.K. Singh, O.P. Pandey, S.K. Sengupta, Spectrochim. Acta. A. 85 (2012) 1–6.
[23] G.B. Bagihalli, P.G. Avaji, S.A. Patil, P.S. Badami, Eur. J. Med. Chem. 43 (2008) 2639–2649.
[24] M.Y. Nassar, I.S. Ahmed, Polyhedron 30 (2011) 2431–2437.
[25] M.Y. Nassar, T.Y. Mohamed, I.S. Ahmed, J. Mol. Struct. 1050 (2013) 81–87.
[26] M.Y. Nassar, I.S. Ahmed, Mater. Res. Bull. 47 (2012) 2638–2645.
[27] M.Y. Nassar, Mater. Lett. 94 (2013) 112–115.
[28] K. Byrappa, A.K. Subramani, S. Ananda, K.M. Lokanatharai, R. Dinesh, M. Yoshimura, Bull. Mater. Sci. 29 (2006) 433–438.
[29] X.T. Zhou, H.B. Ji, X.J. Huang, Molecules. 17 (2012) 1149–1158.
[30] M.Y. Nassar, A.S. Amin, I.S. Ahmed, S. Abdallah, J. Taiwan. Inst. Chem. Eng. 64 (2016) 79–88.
[31] M.Y. Nassar, I.S. Ahmed, T.Y. Mohamed, M. Khatab, RSC Adv. 6 (2016) 20001–20013.
[32] M.Y. Nassar, E.I. Ali, E.S. Zakaria, RSC Adv. 7 (2017) 8034–8050.
[33] M.Y. Nassar, T.Y. Mohamed, I.S. Ahmed, I. Samir, J. Mol. Liq. 225 (2017) 730–740.
[34] M.Y. Nassar, M.M. Moustafa, M.M. Taha, RSC Adv. 6 (2016) 42180–42195.
[35] M.Y. Nassar, S. Abdallah, RSC Adv. 6 (2016) 84050–84067.
[36] M.Y. Nassar, M. Khatab, RSC Adv. 6 (2016) 79688–79705.
[37] M.Y. Nassar, I.S. Ahmed, I. Samir, 131 (2014) 329–334.
[38] M. Mostafa, H.M. Saber, A.A. El-Sadek, M.Y. Nassar, Radiochim. Acta 104 (2016) 257–265.